

Spontaneous spin textures in dipolar spinor condensates

S. Yi^{1,2} and H. Pu¹

¹Department of Physics and Astronomy, and Rice Quantum Institute,
Rice University, Houston, TX 77251-1892, USA and

²Institute of Theoretical Physics, The Chinese Academy of Science, Beijing, 100080, China

(Dated: August 29, 2018)

We have mapped out a detailed phase diagram that shows the ground state structure of a spin-1 condensate with magnetic dipole-dipole interactions. We show that the interplay between the dipolar and the spin-exchange interactions induces a rich variety of quantum phases that exhibit spontaneous magnetic ordering in the form of intricate spin textures.

PACS numbers: 03.75.Mn, 03.75.Gg, 75.45.+j, 75.60.Ej

Recent achievement of chromium condensate provides a platform for exploring the effects of magnetic dipolar interaction in dilute atomic Bose-Einstein condensates (BECs) [1]. On the theoretical side, early studies on dipolar condensates [2, 3] concentrated on the scalar atomic BECs where the dipole moments are assumed to be polarized by, e.g., external magnetic fields. To unlock the magnetic dipole moments, one has to resort to optically confined spinor condensates [4, 5]. A widely used and very powerful theoretical tool in treating spinor condensates is the single mode approximation (SMA) in which different spin states are assumed to share the same spatial wave function [6, 7]. An important implication, as well as a limitation, of the SMA is the lack of spatially varying spin textures, i.e., the spins are uniformly oriented under the SMA. The SMA is, however, expected to be valid only when the total spin-dependent interaction (spin-exchange and dipolar) is sufficiently weak compared to the spin-independent interaction [8], and hence cannot cover the whole spectrum of interesting quantum spin phenomena. The SMA becomes particularly questionable in the presence of dipolar interactions — from the studies of ferromagnetic [9] and ferroelectric [10] materials, it is known that even a relatively weak dipolar interaction may spontaneously induce spatially varying dipole moments, a fact which can be attributed to the long-range anisotropic nature of the dipolar interaction.

In the present work, we investigate the ground state wave function and spin structure of a dipolar spinor condensate by directly minimizing the mean-field energy functional without the assumption of the SMA. The main result is summarized in Fig. 1 where a phase diagram in the parameter space of the relative dipolar strength and the trap aspect ratio is present. It can be seen that the competition between the long-range dipolar and the short-range exchange interactions gives rise to a rich variety of spin textures. These spin textures emerge *spontaneously* in the ground state, in contrast to the case of non-dipolar spinor condensates, where spin textures can only be induced dynamically [11, 12, 13].

We consider an $F = 1$ condensate with three magnetic sublevels $m_F = 1, 0, -1$. In the mean-field treatment, the grand-canonical energy functional of the system can

be expressed as

$$E[\phi_\alpha] = \int d\mathbf{r} \left[\sum_\alpha \frac{\hbar^2 |\nabla \phi_\alpha|^2}{2m} - \mu n + V n + \frac{c_0 n^2}{2} + \frac{c_2 \mathbf{S}^2}{2} \right] + \frac{c_d}{2} \int \frac{d\mathbf{r} d\mathbf{r}'}{|\mathbf{R}|^3} \left[\mathbf{S}(\mathbf{r}) \cdot \mathbf{S}(\mathbf{r}') - \frac{3 \mathbf{S}(\mathbf{r}) \cdot \mathbf{R} \mathbf{S}(\mathbf{r}') \cdot \mathbf{R}}{|\mathbf{R}|^2} \right],$$

where $\phi_\alpha(\mathbf{r}) = \sqrt{n_\alpha(\mathbf{r})} e^{i\Theta_\alpha(\mathbf{r})}$ is the macroscopic wave function of the $m_F = \alpha$ atoms with n_α being the density and Θ_α being the phase of the component α ; μ is the chemical potential, $n = \sum_\alpha n_\alpha$ the total density, $V = m\omega_0^2(x^2 + y^2 + \lambda^2 z^2)/2$ is trapping potential with λ being the trap aspect ratio, $\mathbf{S} = \sum_{\alpha\beta} \phi_\alpha^* \mathbf{F}_{\alpha\beta} \phi_\beta$ is the density of spin with \mathbf{F} being the angular momentum operator, and $\mathbf{R} = \mathbf{r} - \mathbf{r}'$. The collisional interactions include a spin-independent part $c_0 = 4\pi\hbar^2(a_0 + 2a_2)/(3m)$ and a spin-exchange part $c_2 = 4\pi\hbar^2(a_2 - a_0)/(3m)$ with a_f ($f = 0, 2$) being the s -wave scattering length for two spin-1 atoms in the combined symmetric channel of total spin f [5]. For the two experimentally realized spin-1 condensates ^{87}Rb [14] and ^{23}Na [15], the spin-exchange interactions are ferromagnetic ($c_2 < 0$) and anti-ferromagnetic ($c_2 > 0$), respectively. The strength of the dipolar interaction is characterized by $c_d = \mu_0 \mu_B^2 g_F^2 / (4\pi)$ with μ_0 being the vacuum magnetic permeability, μ_B the Bohr magneton, and g_F the Landé g-factor.

The condensate wave function is found by numerically minimizing the energy functional $E[\phi_\alpha, \phi_\alpha^*]$ subject to the constraint of fixed total number of atoms N using the steepest descent method. In our calculation, we fix the value of c_0 to be positive and choose $c_2/c_0 = -0.01$ and 0.03 for the case of the ferromagnetic and anti-ferromagnetic spin-exchange interaction, respectively. These two ratios correspond to the scattering parameters of ^{87}Rb and ^{23}Na , respectively [16]. To focus on the dipolar effects, we allow c_d to vary and introduce $q \equiv c_d/|c_2| \geq 0$ to measure the relative strength of the dipolar interaction. The trap aspect ratio λ (which is varied between 0.1 and 10 in our calculations) is another control knob that allows us to tune the shape of the condensate and hence the effective dipolar interaction [3, 6]. Finally, in all numerical results presented in this paper, we use $N = 10^5$ and $\omega_0 = 2\pi \times 100\text{Hz}$.

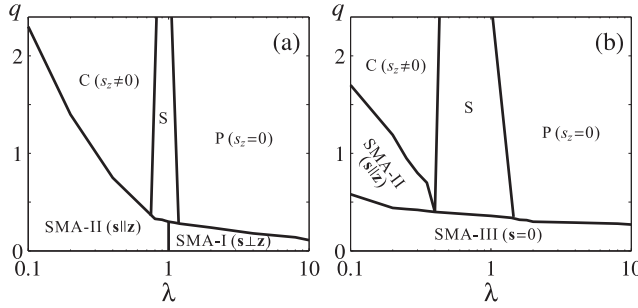


FIG. 1: Phase diagram of dipolar spin-1 condensates of ferromagnetic (a) and anti-ferromagnetic (b) spin-exchange interaction. $\mathbf{s} = \mathbf{S}/n$ is the normalized local spin vector.

Figure 1 summarizes the main result of this paper in the form the phase diagram of the dipolar spin-1 condensate in the q - λ parameter space. For the SMA-I, II, and III phases, the SMA is found to be valid and the spins are uniformly oriented towards a direction determined by the dipolar interaction. In the phases labelled by C, S, and P, the spatial wave functions are spin-dependent and the system exhibits rich spin textures.

SMA ground states — The SMA implies that the normalized local spin vector $\mathbf{s} \equiv \mathbf{S}/n$ is a constant. For a ferromagnetic system in the absence of the dipolar interaction, the vector \mathbf{s} has a length of unity and the ground state is degenerate about the orientation of \mathbf{s} due to the SO(3) symmetry possessed by the order parameter [5]. When the dipolar interaction is present, the SO(3) symmetry is broken and, as shown in Fig. 1(a), the SMA is valid only when q is below a λ -dependent critical value. In the SMA regions, the direction of \mathbf{s} is determined by the trapping geometry: \mathbf{s} is perpendicular to the z -axis for a pancake-shaped ($\lambda > 1$) condensate (SMA-I) and parallel to the z -axis for a cigar-shaped ($\lambda < 1$) condensate (SMA-II), reminiscent of a quantum ferromagnet with easy-plane and easy-axis anisotropy, respectively. This result agrees with the quantum mechanical calculation under the SMA [6].

As shown in Fig. 1(b), for an anti-ferromagnetic system, the SMA is again valid for small q . When q is below a critical value that is rather insensitive to λ , the system exhibits a vanishing spin with $\mathbf{s} = 0$ (SMA-III). For q above this critical value and a cigar-shaped trapping potential with $\lambda \lesssim 0.4$, the dipolar interaction may overwhelm the spin-exchange interaction and make the condensate effectively ferromagnetic, and the system enters the SMA-II phase with spin oriented along the z -axis. We do not find in this case the SMA-I phase with $\mathbf{s} \perp \mathbf{z}$. It is also worth mentioning that transitions between different SMA phases are all first order.

Figure 1 shows that the critical dipolar strength at which the SMA becomes invalid decreases as λ . For a ferromagnetic system, $q_{\text{cr}} = 0.1$ at $\lambda = 10$, which can be reached in ^{87}Rb [6]. The dipolar effects thus become more prominent as the condensate becomes more two-dimensional (2D) pancake-like. This is consistent with

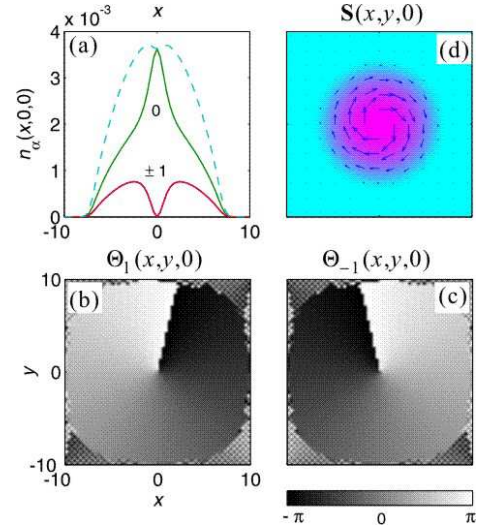


FIG. 2: (Color online). Ground state of the P phase for ferromagnetic coupling with $\lambda = 2$ and $q = 1$. (a) Density of each spin component along the x -axis. The total density is denoted by the dashed line. (b) and (c) are the respective phase images for ϕ_1 and ϕ_{-1} in the $z = 0$ plane. The phase of ϕ_0 is a constant and is not shown here. The phases in the $z \neq 0$ plane are similar. (d) The vector plot of \mathbf{S} in the xy -plane with the color map corresponding to the total density. Here, as well as in Figs. 3 and 4, we adopt $a_{\text{ho}} = (\hbar/m\omega_0)^{1/2}$ and N/a_{ho}^3 as the units for length and density, respectively.

the study in solid magnetic materials, where the dipolar interaction, normally weak enough to be ignored in bulk materials, plays an essential role in stabilizing long-range magnetic order in 2D systems, e.g., in magnetic thin films [17]. Our work shows that it is feasible to observe non-SMA ground state in a pancake ^{87}Rb condensate.

Non-SMA ground states — The SMA regime is analogous to the single-domain regime in micromagnetics, where the exchange energy dominates over all other spin-dependent energy terms and a uniform magnetization forms as a result [9]. As q increases, the SMA eventually breaks down. At large q , the dipolar interaction will dominate the spin-dependent interaction and the difference between the ferromagnetic and anti-ferromagnetic spin-exchange interaction becomes insignificant, as can be seen from Fig. 1. The non-SMA region is further divided into three distinct phases P, C and S, which stands for pancake, cigar and spherical, respectively (see below).

Figure 2 shows a typical wave function in the P phase which occurs in pancake geometry. The density profiles of all spin components are axially symmetric with $n_1(\mathbf{r}) = n_{-1}(\mathbf{r})$ and hence $s_z = 0$, i.e., the spins are planar and lie in the xy -plane. The phases Θ_α take the form

$$\Theta_\alpha = w_\alpha \varphi + \varphi_\alpha, \quad (1)$$

where φ is the azimuthal angle, φ_α is a constant phase that satisfies

$$\varphi_1 + \varphi_{-1} - 2\varphi_0 = 0, \quad (2)$$

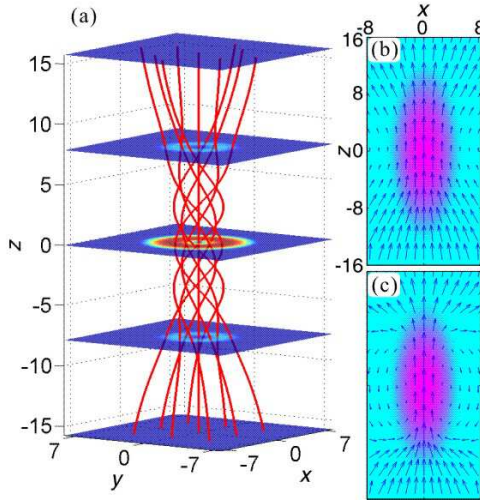


FIG. 3: (Color online). (a) The streamline plot of the spins for ferromagnetic coupling in the C phase with $\lambda = 0.4$ and $q = 1.6$. The color map represents $|\mathbf{S}_\perp|$ on these cross-sections. (b) The vector plot of \mathbf{s}_\parallel in the xz -plane. Same parameters as in (a). (c) The same as (b) except for $q = 6$.

and w_α is the phase winding number with the values

$$\langle w_1, w_0, w_{-1} \rangle = \langle -1, 0, 1 \rangle.$$

Therefore the two spin components, ϕ_1 and ϕ_{-1} , are in vortex states with opposite winding numbers. Due to the presence of the non-rotating ϕ_0 component, the total density does not vanish at the vortex core. Such a ground state represents a coreless skyrmion. It is easy to show that the spin vector can be expressed as

$$\mathbf{S} = 2\sqrt{2n_0n_1} (\sin \varphi, -\cos \varphi, 0).$$

As illustrated in Fig. 2(d), the spin continuously curls around the z -axis to form a vortex such that the system possesses a persistent spin current but no net density current. The spin vortex state is analogous to the flux-closure magnetic states in micromagnetics [9]. In the vicinity of the z -axis, to reduce the exchange energy, the magnitude of the spin gradually decreases and vanishes on the z -axis. This differs from the magnetic vortex observed in nanoscale ferromagnets [18] where, due to the conservation of local spin moment, the magnetization in the vortex core turns toward the z -axis [9].

In the C phase which occurs in a cigar-shaped trap, n_α remains to be cylindrically symmetric and Θ_α can also be expressed in the form of Eq. (1) where the phases φ_α are now z -dependent but still satisfy Eq. (2), and the winding numbers are now given by

$$\langle w_1, w_0, w_{-1} \rangle = \langle 0, 1, 2 \rangle.$$

The spin vector in the C phase takes the form

$$\mathbf{S} = [\Delta \sin(\varphi + \delta), -\Delta \cos(\varphi + \delta), n_1 - n_{-1}],$$

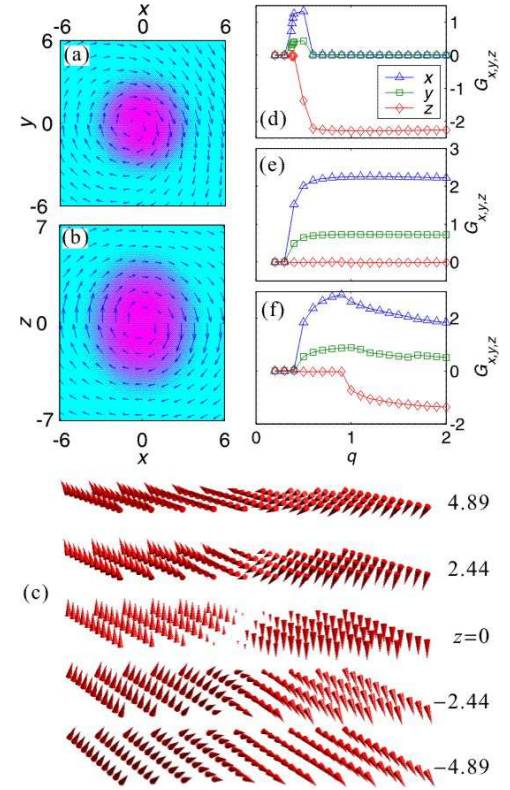


FIG. 4: (Color online). The spin structure in the S phase for anti-ferromagnetic coupling. (a) Spin projection in the $z = 2.29$ plane. $\lambda = 0.4$ and $q = 1$. (b) Spin projection in the $y = 0$ plane. $\lambda = 0.8$ and $q = 1$. (c) The spin structure for $\lambda = 0.8$ and $q = 1$. (d)-(f) The dipolar strength dependence of the toroidal moments for $\lambda = 1.2, 0.8$, and 0.4 , respectively.

where $\Delta \equiv \sqrt{2n_0}(\sqrt{n_1} + \sqrt{n_{-1}})$, and $\delta(z) \equiv \varphi_0(z) - \varphi_1(z)$ is the spin twisting angle which is a monotonically increasing function of z with $\delta(z = 0) = 0$. A typical spin texture plot in the C phase is shown in Fig. 3(a) where one can see that the spins twist around the z -axis, tracing out a helical pattern. The total twisting angle $\delta(\infty) - \delta(-\infty)$ increases with q and approaches π at large q . The corresponding structures of the planar spin $\mathbf{S}_\parallel \equiv (S_x, S_z)$ are plotted in Fig. 3(b) and (c), which resembles the magnetization of a bar magnet. Note that, in the absence of the spin-exchange interaction ($c_2 = 0$), the C phase does not exist and is replaced by the SMA-II phase with spins uniformly oriented along z .

In between the P and C phases, is the S phase which occurs when the trapping potential is close to spherical ($\lambda \approx 1$). A distinct feature of the S phase is that n_α becomes non-axisymmetric, signalling the broken of the cylindrical symmetry of the spatial wave functions. To further quantify the spin texture, we define the spin toroidal moment vector as [10]

$$\mathbf{G} \equiv \int d\mathbf{r} [\mathbf{r} \times \mathbf{S}(\mathbf{r})].$$

For all the SMA phases, we have $\mathbf{G} = 0$. For both the P

and C phases, \mathbf{G} points along the z -axis. The S phase, by contrast, features finite G_x and G_y . The toroidal moments as functions of q is plotted in Fig. 4(d)-(f) for three different values of λ . For small q , $\mathbf{G} = 0$ and the system is in the SMA regime. As q exceeds a threshold, $\mathbf{G} \neq 0$ and the S phase is reached. The continuity of \mathbf{G} suggests, in this mean-field calculation, the transitions between SMA and non-SMA, and also among non-SMA, phases are of second order. In Fig. 4(d), we also see that for $q > 0.6$, the system enters the P phase. Fig. 4(a)-(c) show examples of the spin structure in the S phase. For this particular set of parameters, the condensate displays two domains: one has $S_z > 0$ and the other $S_z < 0$.

Collapse — Condensate collapse will occur when the dipolar interaction strength exceeds a critical value c_d^* . For both ferromagnetic and anti-ferromagnetic coupling, we have found that $c_d^* \approx 0.24c_0$ and is nearly independent of the trap aspect ratio λ . This critical value agrees with that of a highly elongated dipolar scalar condensate with dipole moments polarized along the axial direction [2]. As is well known, the critical dipolar strength for scalar condensate is very sensitive to λ [2]. In the spinor system studied here, the dipoles are free to rearrange themselves to minimize the dipolar interaction, which renders the insensitivity of c_d^* with respect to the trapping geometry.

Dipole induced spin-orbital coupling — In the SMA regime, the total orbital angular momentum \mathbf{L} vanishes, and the ground state wave functions ϕ_α can be taken to be real. In the non-SMA regime, the spin and orbital degrees of freedom are intimately coupled and ϕ_α must be described by complex functions. Here the spin (\mathbf{S}^2) and orbital (\mathbf{L}^2) angular momenta are not separately conserved, only the total angular momentum $(\mathbf{S} + \mathbf{L})^2$ is conserved. It is not difficult to show that, in the non-SMA regime, if the set of wave functions $\{\phi_\alpha\}$ minimizes the energy functional, then the set $\{\phi_\alpha^*\}$ does

not. On the other hand, if we make the transformation: $(\phi_1, \phi_0, \phi_{-1}) \rightarrow (\phi_{-1}^*, -\phi_0^*, \phi_1^*)$, then the new set still minimizes the energy. The above transformation amounts to inverting \mathbf{S} and \mathbf{L} *simultaneously* and hence preserving the relative orientation between them. This inter-connection between \mathbf{S} and \mathbf{L} is well known in superfluid ^3He and the related phenomenon has been termed the spontaneously broken spin-orbit symmetry [19, 20].

The dipole induced spin-orbital coupling is recently explored theoretically in the dynamics of ^{52}Cr condensate and is predicted to manifest in the Einstein-de Haas effect [21]. ^{52}Cr atom features a spin-3 ground state [22] whose short-range collisional interaction is characterized by four scattering lengths and not all of them are accurately known. Although we have studied, in this work, a relatively simpler spin-1 system, we expect much of the essential physics can be applied to higher spin systems.

In conclusion, we have provided a detailed phase diagram which shows the ground state structure of a dipolar spin-1 condensate beyond the SMA. In this system, the spin and orbital degrees of freedom are intimately coupled together. The interplay between the long-range dipolar and the short-range exchange interactions gives rise to a variety of quantum phases characterized by distinctive spin textures. As such, dipolar spinor condensates represent an intriguing quantum magnetic system whose properties are highly tunable. The work here assumes zero magnetic field, an assumption valid for ^{87}Rb and ^{52}Cr when the external magnetic field strength is less than 0.1 mG [6]. This constraint poses an experimental challenge but is definitely within the reach with current technology.

We thank Profs. Michael Chapman, Jason Ho, Carl Rau and Li You, and Dr. Jian Li for many insightful discussions. HP acknowledges the hospitality of the Aspen Center for Physics, and support from ORAU and NSF.

[1] A. Griesmaier *et al.*, Phys. Rev. Lett. **94**, 160401 (2004).
[2] S. Yi and L. You, Phys. Rev. A **61**, 041604(R) (2000); *ibid.* **63**, 053607 (2001); K. Goral *et al.*, *ibid.* **61**, 051601(R) (2000); L. Santos *et al.*, Phys. Rev. Lett. **85**, 1791 (2000).
[3] For a review, see, M. Baranov *et al.*, Phys. Scripta. **T102**, 74 (2002).
[4] D. Stamper-Kurn *et al.*, Phys. Rev. Lett. **80**, 2027 (1998).
[5] T.-L. Ho, Phys. Rev. Lett. **81**, 742 (1998); T. Ohmi and K. Machida, J. Phys. Soc. Jap. **67**, 1822 (1998).
[6] S. Yi, L. You, and H. Pu, Phys. Rev. Lett. **93**, 040403 (2004); S. Yi and H. Pu, Phys. Rev. A **73**, 023602 (2006).
[7] C. K. Law, H. Pu, and N. P. Bigelow, Phys. Rev. Lett. **81**, 5257 (1998).
[8] S. Yi *et al.*, Phys. Rev. A **66**, 011601 (2002).
[9] A. Hubert and R. Schäfer, *Magnetic domains* (Springer, Berlin, 1998).
[10] I. I. Naumov, L. Bellaiche, and H. Fu, Nature (London) **432**, 737 (2004); A. A. Gorbatsevich and Yu. V. Kopaev, Ferroelectrics **161**, 321 (1994).
[11] S.-K. Yip, Phys. Rev. Lett. **83**, 4677 (1999); T. Mizushima, K. Machida, and T. Kita, *ibid.* **89**, 030401 (2002); E. N. Bulgakov and A. F. Sadreev, *ibid.* **90**, 200401 (2003).
[12] M. R. Matthews *et al.*, Phys. Rev. Lett. **83**, 2498 (1999); A. E. Leanhardt *et al.*, *ibid.* **90**, 140403 (2003).
[13] H. T. C. Stoof, E. Vliegen, and U. Al Khawaja, Phys. Rev. Lett. **87**, 120407 (2001); J. Ruostekoski and J. R. Anglin, Phys. Rev. Lett. **91**, 190402 (2003); H. Zhai *et al.*, Phys. Rev. A **68**, 043602 (2003).
[14] M. D. Barret, J. A. Sauer, and M. S. Chapman, Phys. Rev. Lett. **87**, 010404 (2001).
[15] D. M. Stamper-Kurn *et al.*, Phys. Rev. Lett. **80**, 2027 (1998); J. Stenger *et al.*, Nature (London) **396**, 345 (1998).
[16] E.G.M. van Kempen *et al.*, Phys. Rev. Lett. **88**, 093201 (2002); A. Crubellier *et al.*, Eur. Phys. J. D **6**, 211 (1999).
[17] K. De'Bell, A. B. MacIsaac and J. P. Whitehead, Rev. Mod. Phys. **72**, 225 (2000).
[18] K. Bussmann *et al.*, Appl. Phys. Lett. **75**, 2476 (1999); J.

Raabe *et al.*, J. Appl. Phys. **88**, 4437 (2000); T. Shinjo *et al.*, Science **289**, 930 (2000); A. Wachowiak *et al.*, Science **298**, 577 (2002).

[19] D. Vollhardt and P. Wölfle, *The superfluid phases of Helium 3* (Taylor & Francis, London, 1990).

[20] A. J. Leggett, Rev. Mod. Phys. **47**, 331 (1975).

[21] L. Santos and T. Pfau, cond-mat/0510634; Y. Kawaguchi, H. Saito and M. Ueda, Phys. Rev. Lett. **96**, 080405 (2006).

[22] R. B. Diener and T.-L. Ho, cond-mat/0511751.